Electronic Supplementary Information (ESI)

Kinetics of the unimolecular reaction of CH_2OO and the bimolecular reactions with the water monomer, acetaldehyde and acetone at atmospheric conditions

by

Torsten Berndt, Ralf Kaethner, Jens Voigtländer, Frank Stratmann, Mark Pfeifle, Patrick Reichle, Mikko Sipilä, Markku Kulmala and Matthias Olzmann

CFD modelling

To describe the flow, heat and mass transfer (including chemical reactions), in the utilized flow system, numerical simulations were carried out with the commercially available computational fluid dynamics (CFD) software Fluent.[1] Thereby two different geometries (scales), i.e., the free jet flow reactor, and the SO_2 injector, were simulated separately. For both simulations, the numerical resolution grid was chosen such that the requirements of the applied realizable k-epsilon (k-e) turbulence model were fulfilled.[2,3]

For the description of H_2SO_4 formation from $CH_2OO + SO_2$ in the sampling inlet, the chemical reaction scheme was described by the following two equations:

$$CH_2OO + SO_2 \rightarrow SO_3 + HCHO \quad \text{(S1)}$$

$$SO_3 + 2\,H_2O \rightarrow H_2SO_4 + H_2O \quad \text{(S2)}$$

In the simulations, wall losses of SO_3 and H_2SO_4 were taken into account. In more detail, the tube wall was assumed to be an infinite sink for these substances, i.e. the corresponding mass fractions were set to zero at the wall. For all other substances, zero flux wall boundary conditions, implying no losses, were used. The molecular diffusion of the gas mixture, important to calculate the transport processes downstream of the free jet, was treated as multicomponent diffusion. All binary diffusion coefficients were estimated by the method of Tucker and Nelken[4].

Modelling results for the free-jet flow systems are depicted in Fig.1 in the main text and in Fig.S1 showing the centre line concentrations of ozone and TME as a function of time. In Fig.S2 results of an example of the modelling of the CH_2OO conversion by SO_2 and water vapour to H_2SO_4 according to

the reactions (S1) and (S2). A H_2SO_4 formation yield of 0.85 with respect to CH_2OO was found caused by dilution through the SO_2 flow and by wall losses of SO_3 and H_2SO_4 in the turbulent mixing zone.

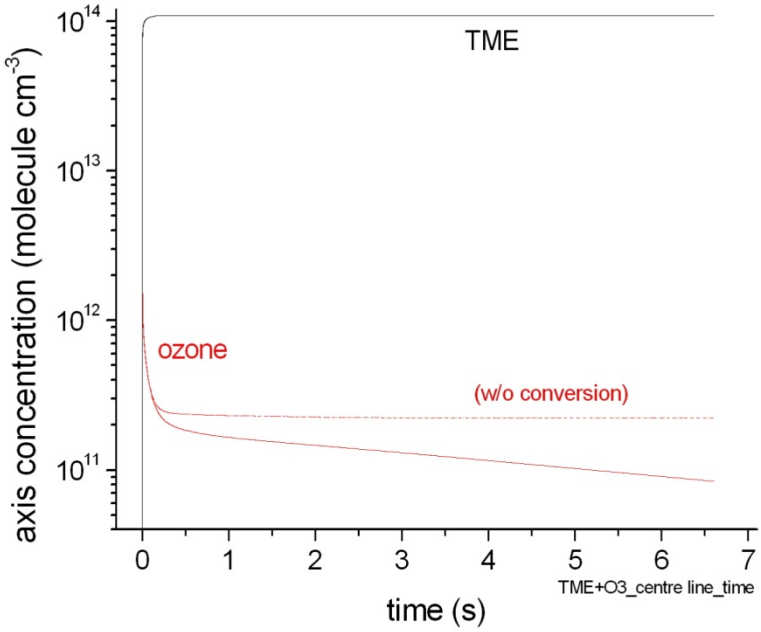

Figure S1: Ozone axis concentration (in red) and TME concentration (in black) as a function of time from CFD modeling of the example run as given in Fig.1 in the main text.

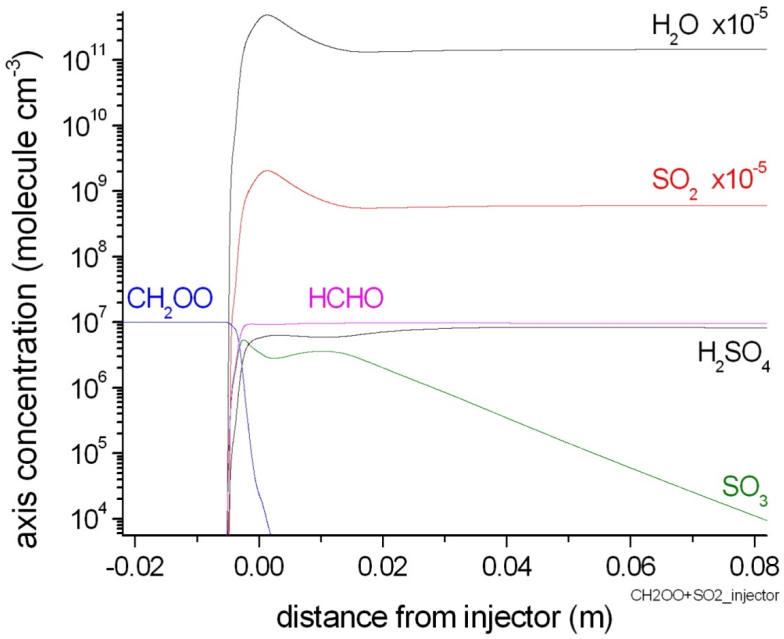

Figure S2: CFD modelling results describing the conversion of CH_2OO (initial concentration: 10^7 molecule cm^{-3}) to H_2SO_4 via the reactions with SO_2 and H_2O. Axis concentrations of reactants and products as a function of the distance from the SO_2/H_2O injector (two opposing nozzles). Wall losses of SO_3 and H_2SO_4 were taken into account. After complete mixing: $[SO_2] = 6.8 \times 10^{13}$ and $[H_2O] \sim 1.5 \times 10^{16}$ molecule cm^{-3}.

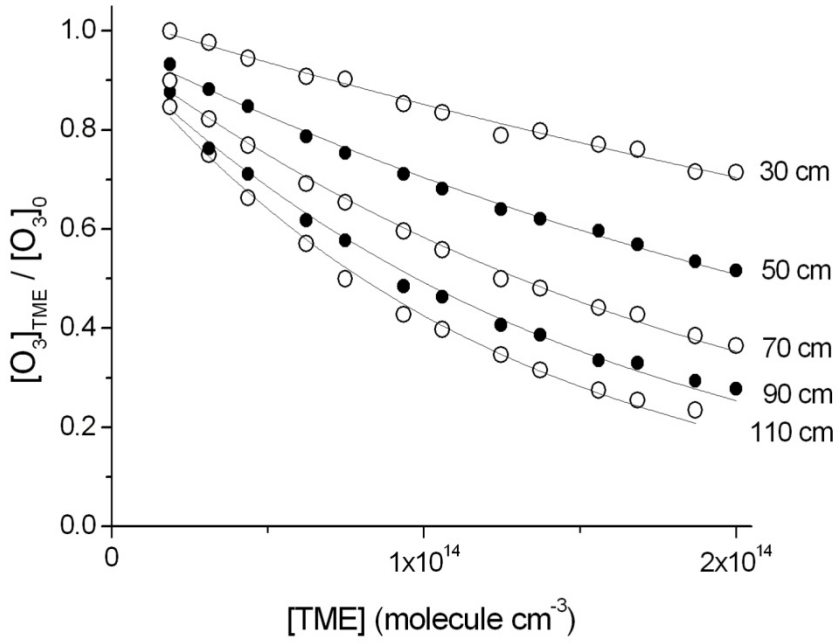

Figure S3: Determination of the reaction time for different distances between nozzle and sampling point (30 – 110 cm) by measuring the ozone disappearance from the reaction with TME using $k_7 = (1.0 \pm 0.2) \times 10^{-15}$ cm^3 molecule^{-1} s^{-1}, $[O_3] = 2.4 \times 10^{11}$ molecule cm^{-3}, [TME] = (1.9 - 20) × 10^{13} molecule cm^{-3}. Lines represent best fit results according to $[O_3]_{TME}/[O_3]_0 = exp(-\ [TME]\ k_7\ t)$.

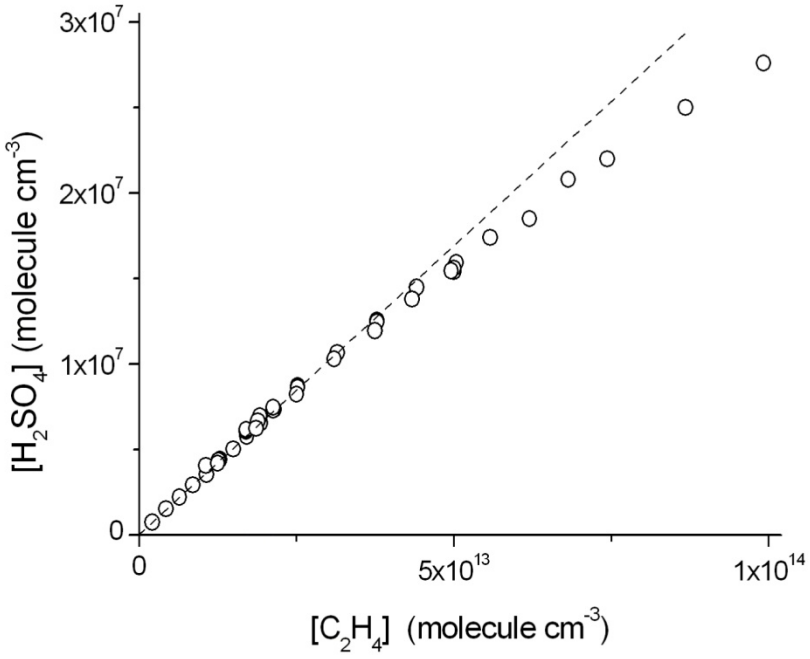

Figure S4: Measured H_2SO_4 concentrations for fixed $[O_3] = 2.3 \times 10^{11}$ molecule cm^{-3} and ethene in the range (2.1 - 99) $\times 10^{12}$ molecule cm^{-3} ; t = 7.5 s and $[C_3H_8] = 7.4 \times 10^{15}$ molecule cm^{-3}.

Upper limit estimate of k($CH_2OO + O_3$)

The experimentally observed deviation from a linear dependence in $[H_2SO_4] = f([O_3])$ for elevated ozone concentrations was used for an estimate of the upper limit of k($CH_2OO + O_3$) neglecting all other CH_2OO consuming steps, such as CH_2OO self-reaction etc.

Starting from equation (II) from the main text and considering the additional reaction

$$CH_2OO + O_3 \rightarrow \text{products} \qquad \text{(S3)}$$

with $[O_3] >> [CH_2OO]$, equation (SI) follows:

$$[H_2SO_4] = \left\{0.85\,\frac{1 - exp(-\{k_3 + k_{S3}[O_3]\}k_3 t)}{k_3 + k_{S3}[O_3]} + t^{add}\right\} y\, k_5[O_3][C_2H_4] \qquad \text{(SI)}$$

The value $k_{S3} = 8.7 \times 10^{-14}$ cm^3 molecule^{-1} s^{-1} was determined from nonlinear regression analysis beside a second free parameter, $k_5'' = y\ k_5\ [C_2H_4]$. Fixed parameters used in equation (SI) were $k_3 = 0.19$ s^{-1}, t = 7.5 s and $t^{add} = 0.4$ s. The value of k_{S3} can be treated as the upper limit for $k(CH_2OO + O_3)$.

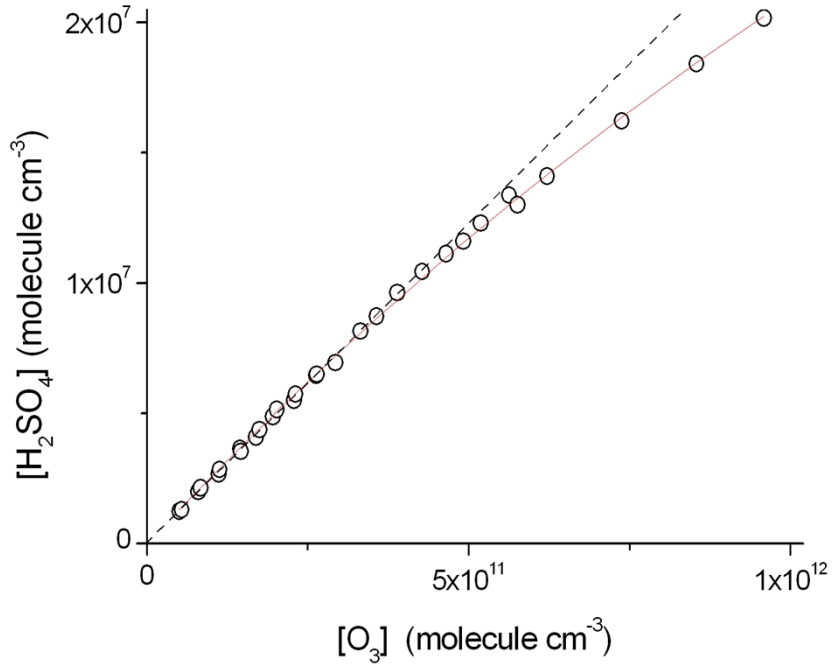

Figure S5: Measured H_2SO_4 concentrations for fixed $[C_2H_4] = 1.86 \times 10^{13}$ molecule cm^{-3} and ozone in the range (5.1 - 96) × 10^{10} molecule cm^{-3} ; t = 7.5 s and $[C_3H_8] = 7.4 \times 10^{15}$ molecule cm^{-3}. The red line shows the result from nonlinear regression analysis, equation (SI).

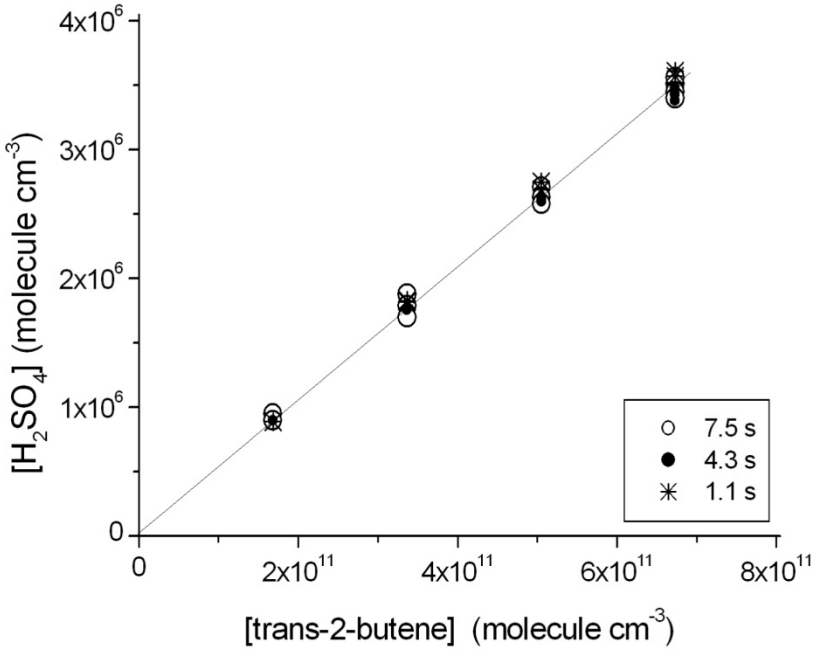

Figure S6: H_2SO_4 concentrations from the ozonolysis of trans-2-butene for different reaction times; $[O_3] = 2.3 \times 10^{11}$, $[C_4H_8] = (1.7 – 6.7) \times 10^{11}$ and $[C_3H_8] = 7.4 \times 10^{15}$ molecule cm^{-3}.

Quantum-chemical calculations

Cartesian coordinates (in Å) at the CCSD(T)/aug-cc-pVTZ level of theory (obtained with Gaussian09[5])

CH_2OO:

C	1.07146100	-0.21852800	0.00000000
H	0.99368300	-1.29927200	0.00000000
H	1.98484500	0.35913500	0.00000000
O	0.00000000	0.47241400	0.00000000
O	-1.17591200	-0.19100000	0.00000000

TS3 (CH_2OO → Dioxirane):

C	0.0001137817	0.0000429712	0.0001135748
H	-0.0004105215	-0.0001249801	1.0893828729
H	0.9098035377	0.0002761698	-0.5868563479
O	-1.1377785248	-0.0719561449	-0.6003101927
O	-0.7601832630	0.9912067340	-1.5415666171

Harmonic vibrational wavenumbers ω_i (unscaled, unit: cm^{-1}) and rotational constants A, B, C (unit: cm^{-1}), CCSD(T)/aug-cc-pVTZ

CH_2OO:

A = 2.5789, B = 0.4145, C = 0.3571

ω_i = (3295, 3135, 1482, 1306, 1230, 933, 855, 616, 529)

TS3:

A = 1.4608, B = 0.5112, C = 0.3950

ω_i = (754i, 3244, 3086, 1517, 1326, 1181, 946, 786, 653)

Details of the single-point energy calculations:

The molecular structures optimized with CCSD(T)/aug-cc-pVTZ were used as a basis for more sophisticated single-point calculations. The relative energies used for the rate coefficient calculations were obtained with the following extrapolation scheme:

$$E = E_{HF}^{\infty} + \Delta E_{CCSD(T)}^{\infty} + \Delta E_{SD(T)\rightarrow SDT(Q)} + f\Delta ZPVE$$

Here, E_{HF}^{∞} is the extrapolated Hartree-Fock energy at the complete basis set (CBS) limit, $\Delta E_{CCSD(T)}^{\infty}$ the corresponding CBS correlation energy at the CCSD(T) (frozen-core) level of theory. For E_{HF}^{∞}, the exponential approach by Feller[6] was chosen, while for $\Delta E_{CCSD(T)}^{\infty}$, a X^{-3} dependence on the cardinal number of the basis set was assumed.[7] For both terms, the three basis sets aug-cc-pVXZ (X = 3(T), 4(Q), 5) were employed. $\Delta E_{SD(T)\rightarrow SDT(Q)}$ represents a correction term for higher-level electron

correlation beyond CCSD(T). It is calculated by the relation $\Delta E_{SD(T)\rightarrow SDT(Q)} = E(CCSDT(Q)/aug-cc-pVDZ) - E(CCSD(T)/aug-cc-pVDZ)$. Finally, $f\Delta ZPVE$ is the scaled harmonic zero-point vibrational energy correction (CCSD(T)/aug-cc-pVTZ). The scaling factor of $f = 0.975$ was adopted from the CCCBDB database[8] and also used to scale the vibrational frequencies for the state-counting routines in the subsequent kinetic calculations. For all coupled cluster calculations, spin-restricted Hartree-Fock (RHF) reference determinants were used.

The model chemistry described above is largely based on the CHEAT1 protocol developed by Faragó et al.[9], albeit higher levels of theory were utilized for all terms in this work. A summary of the differences is presented in Table S1.

Table S1: Comparison of the CHEAT1 protocol and the methodology used in this work.

	CHEAT1[9]	This work
Structures, harmonic frequencies	CCSD/cc-pVTZ	CCSD(T)/aug-cc-pVTZ
E_{HF}^{∞}	aug-cc-pVXZ (X = D, T, Q)	aug-cc-pVXZ (X = T, Q, 5)
$\Delta E_{CCSD(T)}^{\infty}$	aug-cc-pVXZ (X = T, Q), 2-point formula	aug-cc-pVXZ (X = T, Q, 5), least-squares fit
$\Delta E_{SD(T)\rightarrow SDT(Q)}$	cc-pVDZ	aug-cc-pVDZ

The CCSD(T) calculations were performed with the Gaussian09 program package[5], for the CCSDT(Q) energies[10] required for the higher-level correlation term, the MRCC package (version 2014/07/10) was used[11].

Intrinsic reaction coordinate (IRC) for reaction (3)

IRC calculations for the dioxirane formation from CH_2OO (reaction 3) were performed at the CR-CCSD(T)$_L$/aug-cc-pVDZ level of theory[12], as implemented in the GAMESS program package (version 2013/05/01, R1)[13]. The results are shown in Fig. S7 together with the IRC curve at the B3LYP/6-311G(d,p) level of theory (Gaussian09). Both curves are shifted so that the IRC maximum (transition state) coincides with the origin of the coordinate system. As is obvious from the figure, the coupled cluster and B3LYP curves agree well over a large part of the reaction path, with a moderately increasing deviation in going from the transition state towards the Criegee intermediate. The calculation of thermal high-pressure tunneling factors $\Gamma(T)$[14], based on the CR-CCSD(T)$_L$ data, yields values between 2.0 and 1.6 for $T = 270...320\ K$, with $\Gamma(297\ K) = 1.7$. For comparison, the Wigner approximation[15] was also tested for calculating $\Gamma(T)$ (ν_{im} = 754i cm^{-1}), yielding very similar results ($\Gamma(T) = 2.2...1.6$ for $T = 270...320\ K$). Thus, tunneling is not negligible for channel (3a) in the considered temperature range (even though it is not an H transfer reaction).

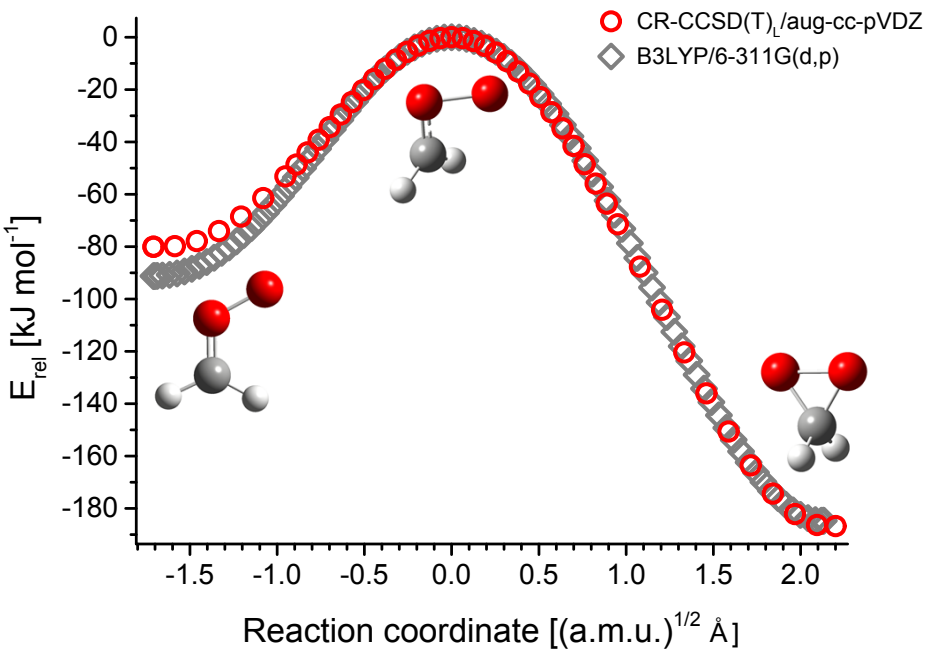

Figure S7: Intrinsic reaction coordinate (IRC) curve for reaction (3)

Details about the master equation calculations

Discretization: $\Delta E_{grain} = 10\ cm^{-1}$, $E_{max} = 20{,}000\ cm^{-1}$ (convergence was checked)

Density of states / sum of states calculation: direct-counting procedures (harmonic oscillator/rigid rotor approximation) based on the Beyer-Swinehart algorithm[16], assuming two quasi-degenerate inactive and one active rotational degree of freedom (K-rotor). $\langle J \rangle = 21$ was used in all calculations (thermally averaged rotational quantum number of CH_2OO at room temperature).

Collision frequency: The following Lennard-Jones parameters were used to calculate the collision frequency:

N_2: $\varepsilon/k_B = 71.4\ K$, $\sigma = 3.798$ Å (Reid et al.[17])

CH_2OO: $\varepsilon/k_B = 520\ K$, $\sigma = 3.79$ Å (see below)

As a model substance for the Criegee intermediate, HCOOH was chosen. Its critical data were obtained from Simmrock et al.[18], and the Lennard-Jones parameters were calculated with the empirical method by Stiel and Thodos[19]. In our master equation model, the bath gas was assumed to be pure N_2 instead of air. This simplification seems justified as the calculated collision frequency for CH_2OO in pure O_2 as a bath gas is only 5% lower than for N_2 at all temperatures considered in our study. Besides the collision frequency, the average energy transferred per collision is expected to be different for N_2 and O_2. However, $\langle \Delta E \rangle_{down}$ is treated as an adjustable parameter anyway and hence a distinction between the two bath gas species is not necessary.

Comparison of the exponential-down and step-ladder models

In the exponential-down model, the probability distribution for deactivating collisions is given by the relation $P_{down}(E,E') = 1/N(E')\exp\left(-\left(E' - E\right)/\alpha\right)$ (see e.g. Holbroock et al.[20]). E' and E are the initial and final energies respectively, α is a parameter that governs the width of the distribution (and therefore the average energy transferred per down collision) and $N(E')$ is a normalization factor. The corresponding distribution for activating collisions, $P_{up}(E,E')$, is determined by detailed balancing. It can be shown that the average energy transferred per stabilizing collision, $\langle\Delta E\rangle_{down}$, is equal to the parameter α for sufficiently high initial energies E'.[20]

In the step-ladder model, $P(E,E') = 0$ for all $E \neq E' \pm \Delta E_{SL}$. $P\left(E' + \Delta E_{SL},E'\right)$ and $P\left(E' - \Delta E_{SL},E'\right)$ are non-zero and can be determined by the normalization condition and the principle of detailed balancing, similar to the exponential-down model. Because the step-ladder model only allows collisions with a fixed amount of transferred energy, it is evident that $\langle\Delta E\rangle_{down} = \Delta E_{SL}$. Thus, master equation calculations with the different models but with $\alpha = \Delta E_{SL}$ are expected to give similar results.

In Table S2, unimolecular rate coefficients $k_3(T,P)$ calculated with both models for exemplary conditions are collected. The agreement between the models is satisfactory as long as the averaged properties of the $P(E,E')$ functions (i.e. $\langle\Delta E\rangle_{down}$) are chosen to be equal. As the numerical master equation solution is considerably faster with the step-ladder model due to its structural simplicity, it was used in the current kinetic investigation.

Table S2: Comparison of $k_3(T,P)$ calculated with the step-ladder and exponential-down model.

ΔE_{SL} or α / cm^{-1}	T / K	P / bar	$k_3(T,P)$/s^{-1}, step-ladder model	$k_3(T,P)$/s^{-1}, exp.-down model
100	270	0.1	8.64×10^{-4}	9.68×10^{-4}
100	270	10	5.49×10^{-3}	5.91×10^{-3}
100	320	0.1	7.68×10^{-2}	9.18×10^{-2}
100	320	10	7.94×10^{-1}	9.08×10^{-1}
500	270	0.1	2.78×10^{-3}	2.24×10^{-3}
500	270	10	9.58×10^{-3}	8.93×10^{-3}
500	320	0.1	3.48×10^{-1}	2.76×10^{-1}
500	320	10	1.90	1.74

References (ESI)

1 Fluent (Ansys Inc., Canonsburg, PA, USA).
2 T.-H. Shih, W. W. Liou, A. Shabbir, Z. Yang, and J. Zhu., *Computers Fluids*, 1995, **24**, 227-238.
3 W. Jones and B. Launder, *Int. J. Heat Mass Transfer*, **15**, 1972, 301-314.
4 W. A. Tucker and L. H. Nelken, Chapter 17, in *Handbook of Chemical Property Estimation Methods*, 1982, eds: W. J. Lyman, W. F. Reehl and D. H. Rosenblatt, American Chemical Society, 1982.
5 M. J. Frisch, G. W. Trucks, H. B. Schlegel, G. E. Scuseria, M. A. Robb, J. R. Cheeseman, G. Scalmani, V. Barone, B. Mennucci, G. A. Petersson, H. Nakatsuji, M. Caricato, X. Li, H. P. Hratchian, A. F. Izmaylov, J. Bloino, G. Zheng, J. L. Sonnenberg, M. Hada, M. Ehara, K. Toyota, R. Fukuda, J. Hasegawa, M. Ishida, T. Nakajima, Y. Honda, O. Kitao, H. Nakai, T. Vreven, J. A. Montgomery, Jr., J. E. Peralta, F. Ogliaro, M. Bearpark, J. J. Heyd, E. Brothers, K. N. Kudin, V. N. Staroverov, R. Kobayashi, J. Normand, K. Raghavachari, A. Rendell, J. C. Burant, S. S. Iyengar, J. Tomasi, M. Cossi, N. Rega, J. M. Millam, M. Klene, J. E. Knox, J. B. Cross, V. Bakken, C. Adamo, J. Jaramillo, R. Gomperts, R. E. Stratmann, O. Yazyev, A. J. Austin, R. Cammi, C. Pomelli, J. W. Ochterski, R. L. Martin, K. Morokuma, V. G. Zakrzewski, G. A. Voth, P. Salvador, J. J. Dannenberg, S. Dapprich, A. D. Daniels, O. Farkas, J. B. Foresman, J. V. Ortiz, J. Cioslowski and D. J. Fox, Gaussian 09, Revision A.02, Gaussian, Inc., Wallingford CT, 2009.
6 D. Feller, *J. Chem. Phys.*, 1993, **98**, 7059-7071.
7 T. Helgaker, W. Klopper, H. Koch and J. Noga, *J. Chem. Phys.*, 1997, **106**, 9639-9646.
8 NIST Computational Chemistry Comparison and Benchmark Database, NIST Standard Reference Database Number 101, Release 16a, August 2013, edited by R. D. Johnson III, http://cccbdb.nist.gov.
9 E. P. Faragó, M. Szőri, M. C. Owen, C. Fittschen, and B. Viskolcz, *J. Chem. Phys.*, 2015, **142**, 054308.
10 Y. J. Bomble, J. F. Stanton, M. Kallay and J. Gauss, *J. Chem. Phys.*, 2005, **123**, 054101.
11 MRCC, a quantum chemical program suite written by M. Kállay, Z. Rolik, I. Ladjánszki, L. Szegedy, B. Ladóczki, J. Csontos, and B. Kornis. See also Z. Rolik, L. Szegedy, I. Ladjánszki, B. Ladóczki and M. Kállay, *J. Chem. Phys.*, 2013, **139**, 094105, as well as: www.mrcc.hu.
12 P. Piecuch and M. Włoch, *J. Chem. Phys.*, 2005, **123**, 224105.
13 M. W. Schmidt, K. K. Baldridge, J. A. Boatz, S. T. Elbert, M. S. Gordon, J. H. Jensen, S. Koseki, N. Matsunaga, K. A. Nguyen, S. Su, T. L. Windus, M. Dupuis, J. A. Montgomery, *J. Comput. Chem.*, 1993, **14**, 1347-1363.
14 B. C. Garrett and D. G. Truhlar, *J. Phys. Chem.*, 1979, **83**, 2921-2926.
15 E. Wigner, *Z. Phys. Chem. B*, 1932, **19**, 203–216.
16 T. Beyer and D. F. Swinehart, *Commun. ACM*, 1973, **16**, 379.
17 R. C. Reid, J. M. Prausnitz and B. E. Poling, *The Properties of Gases and Liquids*, fourth ed., McGraw-Hill, Boston, 1987.
18 K. H. Simmrock, R. Janowsky and A. Ohnsorge, *Critical Data of Pure Substances*, DECHEMA, Frankfurt/Main, Germany, 1996.
19 L. I. Stiel and G. Thodos, *AlChE J.*, 1964, **10**, 266–269.
20 K. A. Holbrook, M. J. Pilling and S. H. Robertson, *Unimolecular Reactions*, second ed., John Wiley & Sons, Chichester, UK, 1996.